LAWRENCE
LIVERMORE
NATIONAL
LABORATORY

LLNL-CONF-401576

Simulation Strategies for Shock-Turbulence Interactions

A. Cook, J. Larsson, W. Cabot, S. K. Lele

February 22, 2008

7th International ERCOFTAC Symposium on Engineering Turbulence
Limassol, Cyprus
June 4, 2008 through June 6, 2008

Disclaimer

SIMULATION STRATEGIES FOR SHOCK-TURBULENCE INTERACTIONS

A. W. Cook[1], *J. Larsson*[2], *W. H. Cabot*[1] *and S. K. Lele*[2]

[1] *Lawrence Livermore National Laboratory, Livermore CA 94551*
[2] *Center for Turbulence Research, Stanford University, Stanford, CA 94305*

awcook@llnl.gov

Abstract

The computational challenge of predicting shock-turbulence interactions stems from the fundamentally different physics at play. Shock waves are microscopically thin regions wherein flow properties change rapidly over a distance roughly equal to the molecular mean free path; hence, they are essentially strong discontinuities in the flow field. Turbulence, on the other hand, is a chaotic phenomenon with broadband spatial and temporal scales of motion. Most shock-capturing methods rely on strong numerical dissipation to artificially smooth the discontinuity, such that it can be resolved on the computational grid. Unfortunately, the artificial dissipation necessary for capturing shocks has a deleterious effect on turbulence. An additional problem is the fact that shock-capturing schemes are typically based on one-dimensional Riemann solutions that are not strictly valid in multiple dimensions. This can lead to anisotropy errors and grid-seeded perturbations. Other complications arising from upwinding, flux limiting, operator splitting etc., can seriously degrade performance and generate significant errors, especially in multiple dimensions. The purpose of this work is to design improved algorithms, capable of capturing both shocks and turbulence, which also scale to tens of thousands of processors. We have evaluated two new hydrodynamic algorithms, in relation to the widely used WENO method, on a suite of test cases. The new methods, referred to as the "Compact" and "Hybrid" schemes, show very promising results.

1 Introduction

The Navier-Stokes equations for compressible flow of an ideal gas, with constant specific heats, are (underline denotes tensor):

$$\dot{\rho} + \nabla \cdot \rho\mathbf{u} = 0 \,, \tag{1}$$

$$\dot{\mathbf{m}} + \nabla \cdot (\rho\mathbf{u}\mathbf{u} + p\underline{\boldsymbol{\delta}} - \underline{\boldsymbol{\tau}}) = 0 \,, \tag{2}$$

$$\dot{E} + \nabla \cdot [E\mathbf{u} + (p\underline{\boldsymbol{\delta}} - \underline{\boldsymbol{\tau}}) \cdot \mathbf{u} + \mathbf{q}] = 0 \,, \tag{3}$$

$$p = (\gamma - 1)\rho e \,, \tag{4}$$

where ρ is density, $\mathbf{u} = (u, v, w)$ is velocity, $\mathbf{m} = \rho\mathbf{u}$ is momentum p is pressure, $\underline{\boldsymbol{\delta}}$ is the unit tensor, $E = \rho(e + \mathbf{u} \cdot \mathbf{u}/2)$ is total energy, e is specific internal energy and $\gamma = c_p/c_v$ is the ratio of specific heats. The viscous stress tensor, $\underline{\boldsymbol{\tau}}$, is given by

$$\underline{\boldsymbol{\tau}} = \mu(2\underline{\mathbf{S}}) + (\beta - \frac{2}{3}\mu)(\nabla \cdot \mathbf{u})\underline{\boldsymbol{\delta}} \,, \tag{5}$$

where μ is dynamic (shear) viscosity, β is bulk viscosity and $\underline{\mathbf{S}}$ is the symmetric strain rate tensor

$$\underline{\mathbf{S}} = \frac{1}{2}(\nabla\mathbf{u} + \mathbf{u}\nabla) \,, \tag{6}$$

where $\mathbf{u}\nabla$ denotes the transpose of $\nabla\mathbf{u}$. The conductive heat flux vector, $\mathbf{q}$, is given by Fourier's law,

$$\mathbf{q} = -\sigma\nabla T \,, \tag{7}$$

where σ is thermal conductivity and $T = (\gamma - 1)e/R$ is temperature (with $R = c_p - c_v$ being the gas constant). These equations contain all the essential physics of flows involving both shocks and turbulence. Direct Numerical Simulations (DNS) of turbulent flows are typically performed by solving (1-7) with spectral (Fourier, Chebyshev or Legendre polynomials) or spectral-like (compact/Padé) methods, because such methods are much better able to resolve a wide range of scales than lower-order finite-difference or finite-volume schemes (Orszag & Patterson, 1972; Gottlieb & Orszag, 1977; Vichnevetsky & Bowles, 1982; Lele, 1992). Flows involving shocks however, are most commonly treated with low-order methods, which either take advantage of the eigenstructure of the equations (Godunov) and/or adjust the local differencing stencil (ENO) to capture discontinuities with minimal oscillations. In many applications, ranging from Inertial Confinement Fusion (ICF) to supernovae, shocks deposit vorticity at material interfaces, which subsequently evolve into turbulent mixing zones; secondary shocks may then pass back through the turbulent regions. Such problems present a formidable challenge to traditional algorithms, where high order of accuracy for turbulent mixing is usually sacrificed in favor of robustness and monotonicity for the shocks. The need for accurate predictions of mixing at shock-accelerated interfaces continues to drive development of high-resolution shock-capturing schemes.

2 Methods

There are basically two strategies for obtaining more accurate solutions to flows involving both shocks and turbulence: a "bottom up" approach, whereby finite-difference schemes are extended to higher order, and a "top down" approach, wherein hyperviscosity and/or low-pass filtering is introduced to spectral-like algorithms to increase their robustness. Our "top down" and "bottom up" approaches here consist of a "Compact" method and a "Hybrid" method. We compare the results both to converged reference solutions and to the results of a 7th-order standard WENO method with Roe flux-splitting (Jiang & Shu, 1996).

The Compact method employs a 10th-order Padé scheme for spatial derivatives combined with a 4th-order Runge-Kutta method for temporal integration. An 8th-order dealiasing filter is applied to the conserved variables following each Runge-Kutta substep. Grid-dependent models are used for μ, β and σ. The artificial fluid properties impart a high-wavenumber bias to the dissipation, approximating the cusp in the Heisenberg-Kraichnan spectral viscosity for isotropic turbulence. Like real fluid properties, the artificial properties are required to be positive definite, frame invariant and carry over to the incompressible limit. Unlike real fluid properties, the artificial properties are designed to vanish in smooth regions, while providing strong damping near discontinuities. The method is described in detail by Cook (2007).

The Hybrid method is based on the idea that broadband turbulence and discontinuities represent different physics and thus should be treated by different numerical methods. It consists of essentially three components that can be chosen rather freely: a central finite-difference scheme for the smooth regions, a shock-capturing scheme for the regions containing discontinuities, and a solution-adaptive sensor which identifies these regions. For shock-capturing, a 7th-order WENO method (Jiang & Shu, 1996) is chosen due to its ability to capture shocks in a sharp fashion with few adjustable parameters. Away from the shocks, an 8th-order central difference scheme is used on a split form of the convective terms that improves nonlinear stability. These schemes are coupled in a conservative manner that preserves stability (Larsson & Gustafsson, 2008). The shock sensor is inspired by the observation that shock waves are associated with large negative dilatation, whereas turbulence is more typically associated with large vorticity. Comparing these quantities then yields an effective shock sensor. In 1D, where the vorticity is zero, the density-based sensor by Hill & Pullin, (2004) is used instead. The primary advantage of the Hybrid approach, as compared to a 'shock-capturing only' method, is that numerical dissipation is restricted to the regions flagged by the sensor, which may improve predictions of turbulence spectra. Another advantage is a lowered computational cost, because the more expensive shock-capturing scheme is used in only small parts of the domain. The main drawback is the reliance on the sensor to correctly identify the shocks.

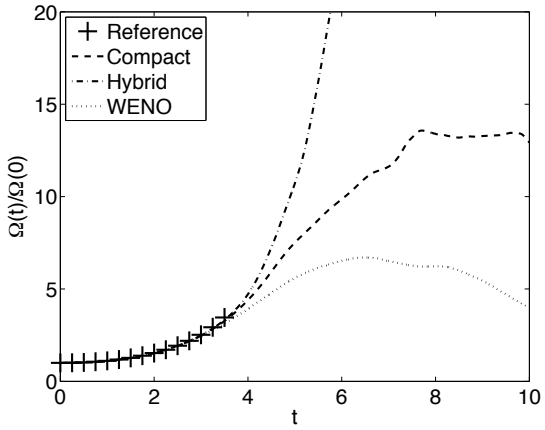

Figure 1: Normalized enstrophy versus time for the Taylor-Green vortex. Simulations were conducted in a $2\pi^3$ periodic box using 64^3 grid points. The reference points correspond to the analytical solution.

3 Taylor-Green Vortex

As a first point of comparison, we consider the inviscid Taylor-Green vortex (Taylor & Green, 1937), which provides an effective test of each schemes' ability to resolve small-scale turbulence. The initial conditions are:

$$\begin{aligned}
\rho &= 1 \,, \\
u &= \sin(x)\cos(y)\cos(z) \,, \\
v &= -\cos(x)\sin(y)\cos(z) \,, \\
w &= 0 \,, \\
p &= \{[\cos(2z)+2][\cos(2x)+\cos(2y)]-2\}/16 \\
&\quad + 100 \,, \\
\gamma &= 5/3 \,.
\end{aligned}$$

The constant of 100 is selected to make the Mach number very low, such that the incompressible solution (Morf *et al.*, 1980; Brachet *et al.*, 1983) can be used for comparison. As the flow evolves, the vortex stretches and bends, thus broadening the spectrum to include higher wavenumbers. Stretching and bending of vortex lines constitute key energy cascade mechanisms in turbulent flows. The computational domain is a triply-periodic $(2\pi)^3$ box on a 64^3 grid.

Figure 1 shows normalized total enstrophy, i.e., $\Omega(t)/\Omega(0)$, where

$$\Omega(t) \equiv \frac{1}{2}\int_V \boldsymbol{\omega}\cdot\boldsymbol{\omega}\, dV \;,\; \omega = \bigtriangledown \times \mathbf{u} \,.$$

The theoretical result is accurate up to about $t = 3.5$ and is plotted in order to assess the ability of each method to resolve small-scale vortex dynamics.

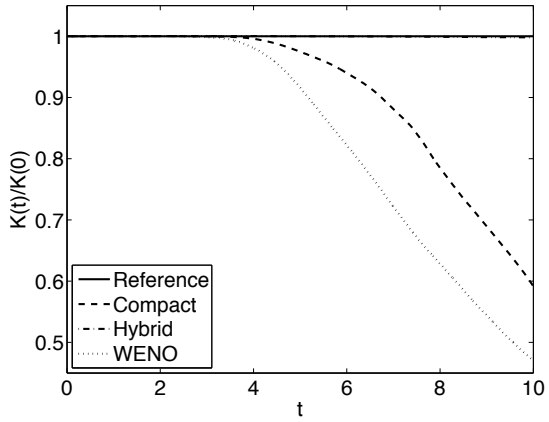

Figure 2: Normalized kinetic energy versus time for the Taylor-Green vortex.

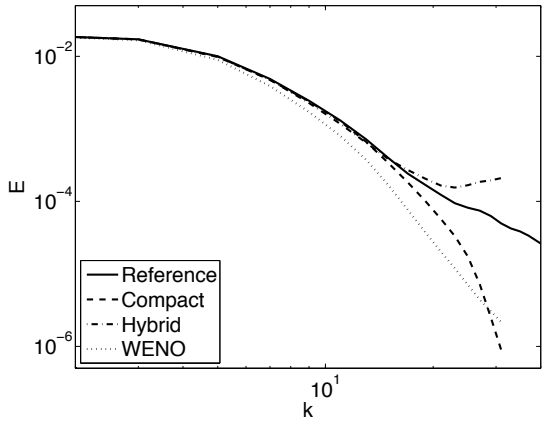

Figure 3: Energy spectrum for Taylor-Green vortex at $t = 5$. The reference spectrum was computed with the Hybrid method at a resolution of 256^3.

Analysis based on Padé approximants and the behavior of the analyticity strip, predicts $\Omega(t)$ will become far too large to capture on a such a coarse grid (Morf *et al.*, 1980); nevertheless, the ability of a scheme to track the enstrophy curve, as well as the maximum enstrophy that a scheme is able to generate, provide stringent tests of resolving power. The Hybrid and Compact methods are much better at tracking small-scale vorticity than the WENO method.

In addition to total enstrophy, the evolution of kinetic energy provides insight into the resolving power of numerical algorithms. Normalized kinetic energy, $K(t)/K(0)$, is plotted for each scheme in Fig. 2, where

$$K(t) \equiv \frac{1}{2}\int_V \rho\,\mathbf{u}\cdot\mathbf{u}\,dV\ .$$

The drop-off in energy for the WENO and Compact schemes results from transfer to unresolved wavenumbers. Energy cascading to scales below 2Δ must be removed to prevent it from piling up near the Nyquist limit. If the energy is not removed, then unphysical ringing begins to appear; i.e., strong point-to-point oscillations propagate throughout the domain and the spectrum approaches a k^2 power law at higher wavenumbers. This is illustrated in Fig. 3, where the spectrum of turbulent kinetic energy is plotted for each method. By $t = 5$, some of the kinetic energy has reached unresolved wavenumbers. For the Hybrid scheme, the sensor detects no shocks; hence, the method defaults to purely centered derivatives everywhere. Centered derivatives are non-dissipative; thus, the method conserves kinetic energy, which causes the spectrum to curl up at higher wavenumbers. The filter and artificial viscosity in the Compact scheme remove high-wavenumber energy in order to reduce aliasing errors; this causes the tail of the spectrum to drop off.

4 Shu-Osher problem

As a second point of comparison, we consider the Shu-Osher problem (Shu & Osher, 1989), which tests each schemes' ability to capture shocks in nonuniform fields. This flow is a canonical model of a one-dimensional shock-turbulence interaction. The nondimensional initial conditions are:

$$\begin{aligned}
&\gamma = 1.4\\
&\text{for } x < -4:\\
&\quad \rho = 3.857143\ ,\ p = 10.33333\ ,\ u = 2.629369\\
&\text{for } x \geq -4:\\
&\quad \rho = 1 + 0.2\sin(5x)\ ,\ p = 1\ ,\ u = 0\ .
\end{aligned}$$

As the shock propagates into the sinusoidal density field, it leaves a steeply undulating flow in the post-shock region. Figures 4 and 5 display the entropy and density solutions for the shock profile as well as the post-shock oscillations. In this case, the sensor in the Hybrid method switches to a more dissipative WENO scheme at the shock. Dissipation in the Compact scheme is primarily accomplished through an artificial bulk viscosity. It is instructive to compare the entropy fields for the Hybrid and pure WENO methods. At the shock they both rely on the same WENO scheme, and there the entropy profiles agree. The entropy waves farther to the left in the figure were generated at earlier times, and there the numerical dissipation of the WENO scheme causes the waves to decay rapidly. The Hybrid method switches back to a central scheme and does not suffer from this effect.

5 Compressible Turbulence

Finally, we consider compressible isotropic turbulence with a turbulent Mach number $M_t = \sqrt{3}u_{\rm rms}/c = 0.6$, which is high enough for the turbulence to spontaneously produce eddy shocklets. We note that these eddy shocklets are strong enough to cause rapid blow-up of the simulations in the absence of any shock-capturing dissipation. The initial con-

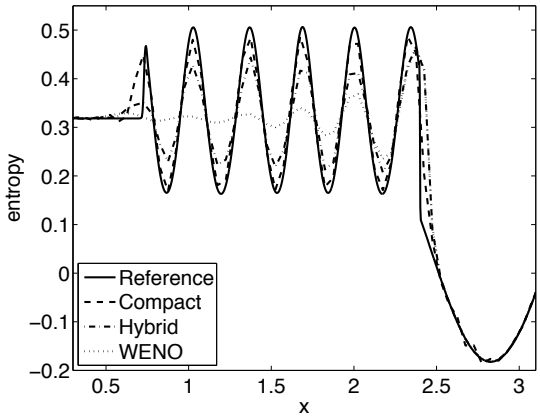

Figure 4: Entropy curves from the Shu-Osher problem at $t = 1.8$. The black line is the converged solution using the Hybrid method with a grid spacing of $\Delta = 10/3200$. The other curves were obtained from simulations using a grid spacing of $\Delta = 10/200$.

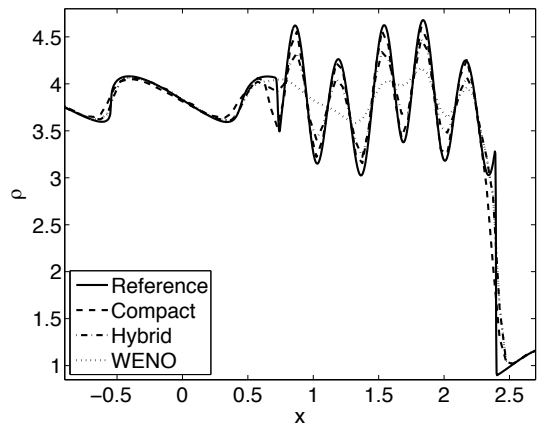

Figure 5: Density curves from the Shu-Osher problem at $t = 1.8$. The black line is the converged solution using the Hybrid method with a grid spacing of $\Delta = 10/3200$. The other curves were obtained from simulations using a grid spacing of $\Delta = 10/200$.

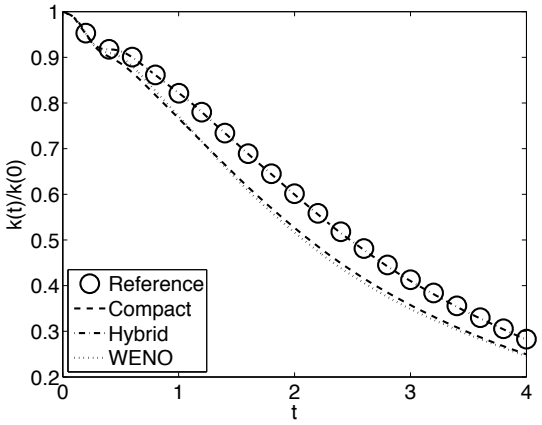

Figure 6: Temporal evolution of normalized velocity variance on 64^3 grids compared to the filtered Hybrid solution on a 256^3 grid.

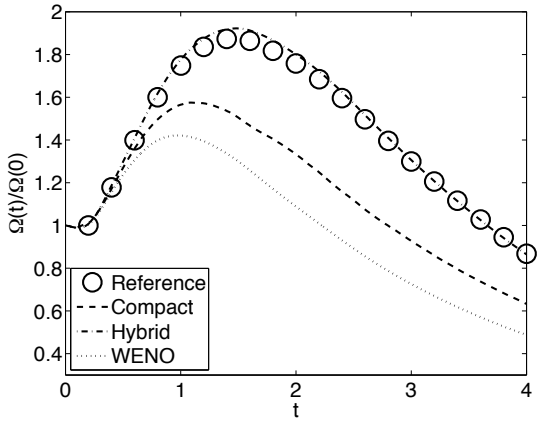

Figure 7: Temporal evolution of normalized enstrophy on 64^3 grids compared to the filtered Hybrid solution on a 256^3 grid.

dition is a randomized velocity field with spectrum $E(k) \sim k^4 \exp(-2k/k_0^2)$ with $k_0 = 4$. The temporal decay of the velocity variance defined by

$$k(t) \equiv \frac{1}{2} \int_V \mathbf{u} \cdot \mathbf{u} \, dV \, .$$

is shown in Fig. 6, while that of the enstrophy is shown in Fig. 7. The dilatation-based shock sensor in the Hybrid method is well adapted to this problem, with the WENO scheme being used in about 1% of the grid points. This explains the relatively low amount of numerical dissipation for the Hybrid method compared to pure WENO. The Compact results fall in between the reference and WENO results. The spectra of vorticity at the end of the simulations (after 4 eddy turn-over times) are shown in Fig. 8. The shapes of the WENO and Compact spectra are slightly different; i.e., dissipation in the Compact method is weighted towards higher wavenumbers.

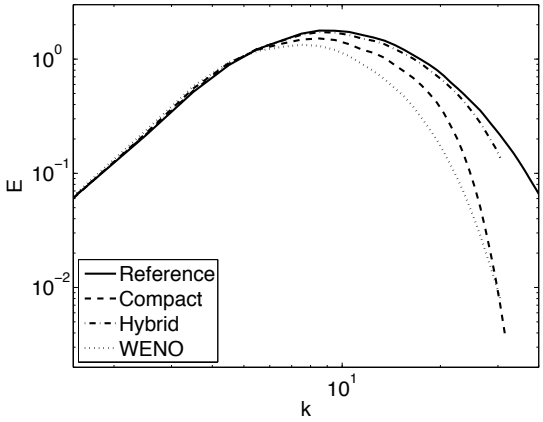

Figure 8: Vorticity spectra at $t = 4$ from 64^3 simulations of decaying compressible isotropic turbulence compared to Hybrid results on a 256^3 grid.

Snapshots of instantaneous dilatation and vorticity are shown in Fig. 9 for the three methods, along with the reference Hybrid results on a 256^3 grid. We first note that the solutions are broadly similar, despite the chaotic nature of the problem and the inherent sensitive dependence on initial conditions. The snapshots of vorticity magnitude illustrate what the previous figures showed statistically; i.e., that the WENO method yields an overly smooth solution with too large dissipation of the smallest scales, while the Hybrid and Compact methods better preserve these finer motions.

The reference snapshot of negative dilatation shows an eddy shocklet with intense compression near the center of the frame. This shocklet is visible in the coarse-grid Hybrid result as well, and to a lesser degree also in the WENO result. Since the Hybrid method uses exactly the same WENO scheme around the shocklet, the difference between these two methods must stem from differences away from the shocklet at earlier times. The Compact method at 256^3 resolution (not shown) exhibits structures very similar to the Hybrid results; however, at 64^3 resolution, the Compact method yields a very smooth dilatation field. This behavior is the subject of ongoing investigations.

6 Conclusions

The results presented herein provide a small sample of the differences between standard WENO, a Hybrid method and a Compact scheme applied to problems involving both shocks and turbulence. While not shown here, we note that both the Hybrid and Compact methods are capable of capturing exceedingly strong shocks, with very little difference in shock thickness. Overall, the Hybrid and Compact schemes outperform the standard WENO method, providing lower inherent numerical dissipation and better resolution of small-scale vorticity. Hence both methods appear better suited to detailed studies of shock/turbulence interaction problems.

Acknowledgments

This work was partially prepared by LLNL under Contract DE-AC52-07NA27344. Support from SciDAC DOE grant DE-FC02-06-ER25787 is gratefully acknowledged, along with support from the Natural Sciences and Engineering Research Council of Canada.

References

BRACHET, M. E., MEIRON, D. I., ORSZAG, S. A., NICKEL, B. G., MORF, R. H. & FRISCH, U. 1983 Small-scale structure of the Taylor-Green vortex. *J. Fluid Mech.* **130**, 411–452.

COOK, A. W. 2007 Artificial fluid properties for large-eddy simulation of compressible turbulent mixing. *Phys. Fluids* **19**, 055103.

GOTTLIEB, D. & ORSZAG, S. A. 1977 *Numerical Analysis of Spectral Methods*. Montpelier: Capital City Press.

HILL, D. J. & PULLIN, D. I. 2004 Hybrid tuned center-difference-WENO method for large eddy simulation in the presence of strong shocks. *J. Comput. Phys.* **194**, 435–450.

JIANG, G.-S. & SHU, C.-W. 1996 Efficient implementation of weighted ENO schemes. *J. Comput. Phys.* **126**, 202–228.

LARSSON, J. & GUSTAFSSON, B. 2008 Stability criteria for hybrid difference methods. *J. Comput. Phys.* **227**, 2886–2898.

LELE, S. K. 1992 Compact finite difference schemes with spectral-like resolution. *J. Comput. Phys.* **103**, 16–42.

MORF, R. H., ORSZAG, S. A. & FRISCH, U. 1980 Spontaneous singularity in three-dimensional, inviscid, incompressible flow. *Phys. Rev. Lett.* **44**, 572–575.

ORSZAG, S. A. & PATTERSON, G. S. 1972 Numerical simulation of three-dimensional homogeneous isotropic turbulence. *Phys. Rev. Lett.* **28**, 76–79.

SHU, C.-W. & OSHER, S. J. 1989 Efficient implementation of essentially non-oscillatory shock capturing schemes II. *J. Comput. Phys.* **83**, 32–78.

TAYLOR, G. I. & GREEN, A. E. 1937 Mechanism of the production of small eddies from large ones. *Proc. Roy. Soc. A* **158**, 499–521.

VICHNEVETSKY, R. & BOWLES, J. B. 1982 *Fourier Analysis of Numerical Approximations of Hyperbolic Equations*. Philadelphia: SIAM.

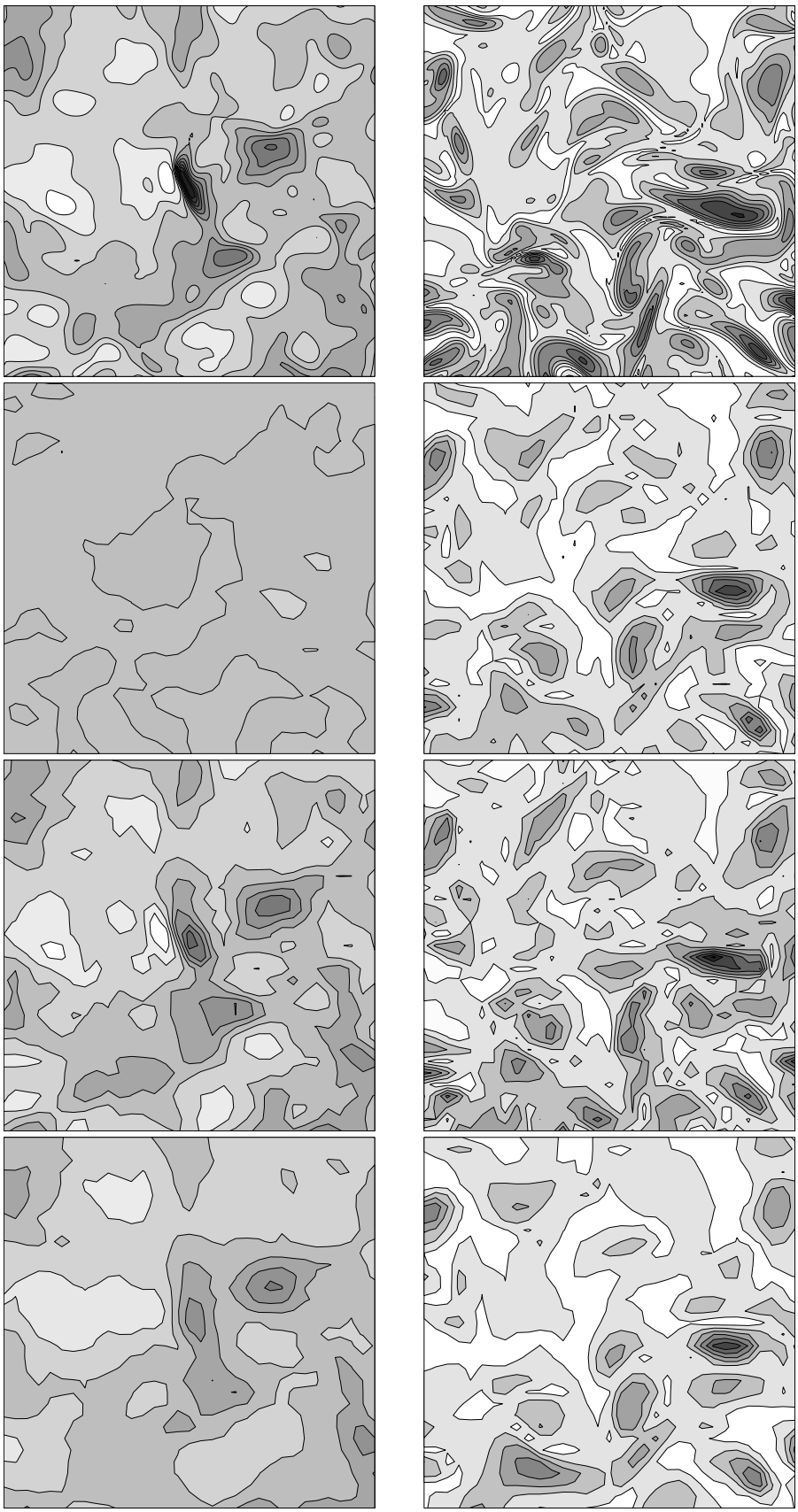

Figure 9: Snapshots at $t = 4$ from 64^3 simulations of decaying compressible isotropic turbulence. Negative dilatation (left column) and vorticity magnitude (right column). From top to bottom, using the same gray-scale maps: 256^3 Hybrid, Compact, Hybrid, and WENO.